PHYSICAL REVIEW FLUIDS **2**, 012501(R) (2017)

Relative role of convective and diffusive mixing in the miscible Rayleigh-Taylor instability in porous media

S. S. Gopalakrishnan,[1,2] J. Carballido-Landeira,[1] A. De Wit,[1] and B. Knaepen[2]
[1]*Université libre de Bruxelles (ULB), Nonlinear Physical Chemistry Unit, CP231, 1050, Brussels, Belgium*
[2]*Université libre de Bruxelles (ULB), Service de Physique Statistique et des Plasmas, CP231, 1050, Brussels, Belgium*
(Received 11 March 2016; published 13 January 2017)

The relative role of convection and diffusion is characterized both numerically and experimentally for porous media flows due to a Rayleigh-Taylor instability of a horizontal interface between two miscible solutions in the gravity field. We show that, though globally convection dominates over diffusion during the nonlinear regime, diffusion can locally be as important as convection and even dominates over lateral convection far away from the fingertips. Our experimental and numerical computations of the temporal evolution of the mixing length, the width of the fingers, and their wavelength are in good agreement and show that the lateral evolution of fingers is governed by diffusion.

DOI: 10.1103/PhysRevFluids.2.012501

The search for scaling laws in hydrodynamics, aimed towards characterizing generic properties of flow dynamics, is ubiquitous and flows in porous media are no exception [1–9]. Understanding scalings for convective processes in porous media is important in applications such as carbon-dioxide (CO_2) sequestration [3,4,9,10], planetary dynamics and formation of stars [11], plasma fusion reactors [12], etc. For these and various other geological and industrial settings, predicting scalings in the evolution of buoyancy-driven patterns at the interface between two solutions plays a pivotal role in predicting mass transport phenomena. Density-driven instabilities can arise, for instance, thanks to a Rayleigh-Taylor (RT) instability developing when a denser solution is placed above a less dense one in the gravity field, or because of double-diffusive effects when solutions of two solutes diffusing at different rates are in contact. In the nonlinear regimes of these instabilities, quantifying the relative importance of convection and diffusion is a prerequisite to analyzing local mass fluxes and hence the efficiency of transport and local mixing.

For porous media, the various dynamical regimes appearing in buoyancy-driven fingering have been studied extensively [2,3,13–18]. In the case of a RT instability of a miscible interface, there is initially a diffusive regime in which the perturbations decay exponentially around the initially flat contact line between the two solutions. Subsequently, perturbations grow in magnitude, triggering convective fingers, and eventually the dynamics enter into a nonlinear regime. This phase is characterized by interactions among the fingers, and an increase in time of the length of the mixing zone that deviates from $t^{1/2}$. During this nonlinear regime, the dynamics is usually considered to be globally dominated by convection, with diffusion being negligible [2,4] even though the rate of growth of the width of fingers has been observed numerically to scale as $t^{1/2}$ [3,4].

Despite this globally satisfying picture, several questions remain unanswered. First, the argument that the nonlinear dynamics is dominated by convection, with diffusion being negligible, has not yet been formally verified. If the contribution of the convective and diffusive terms are monitored globally, it is indeed true that during the initial stages diffusion is dominant and that convective mixing takes over after the onset of instability. However, such an analysis provides an incomplete picture, since both convective and diffusive mixing are significant even during the nonlinear regime, albeit in different regions of the flow. As we highlight below, convection dominates locally at the tip of the fingers but is balanced by diffusion in the rest of the mixing zone. Second, while the dominant vertical length scale of the fingers is well characterized, less is known about horizontal scalings.

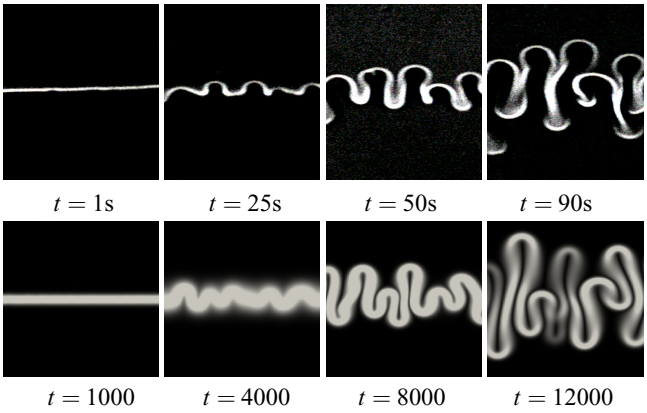

FIG. 1. Buoyancy-driven instabilities: (top) gradients of refractive index in experiments using a sucrose solution (solutal expansion coefficient $\alpha_A = 0.122$ l/mol, diffusion coefficient $D_A = 0.52 \times 10^{-5}$ cm^2/s) with $A_t = 0.0057$M, $A_b = 0.00082$M; (bottom) numerical density gradients. The fields of view in both images correspond to 11 mm $\times$ 20 mm.

We show here by combined numerical simulations and experiments on the miscible RT instability that in porous media diffusion can be locally as important as convection. In particular, a horizontal mixing scale distinct from the vertical one emerges, with the width of the fingers evolving as $t^{1/2}$, similar to the case of convective dissolution [3,4], showing the importance of diffusion in quantifying transverse mixing.

Experiments are carried out in vertical Hele-Shaw cells, two transparent glass plates separated by a small gap here of thickness $a = 0.25$ mm [19]. In this gap, two miscible aqueous solutions of the same solute in concentrations A_t (top) and A_b (bottom) are brought in contact along an initially planar interface using a specific injection procedure [20]. The flow dynamics is visualized using a Schlieren technique, tracking gradients of refractive index [21]. A typical experimental example of RT dynamics deforming the interface in fingers growing in the vertical direction is shown in Fig. 1(a) where a denser solution of sucrose is put on top of a less dense one in a Hele-Shaw cell.

For sufficiently small gap widths, the flow evolution in a Hele-Shaw cell is described, as for flows in porous media [22], by Darcy's equations which, in dimensionless variables, read:

$$\nabla p = -\mathbf{u} + A\hat{\mathbf{y}}, \quad \nabla \cdot \mathbf{u} = 0, \quad \partial_t A + \mathbf{u} \cdot \nabla A = \nabla^2 A, \tag{1}$$

where p is the pressure, $\mathbf{u}$ is the velocity, A denotes the concentration of the solute affecting density, and $\hat{\mathbf{y}}$ is the unit vector in the direction of gravity. The equations are nondimensionalized using the characteristic speed related to the strength of buoyancy forces, namely $\mathscr{U} = \alpha_A A_t g K/\nu$, length $\mathscr{L} = D_A\phi/\mathscr{U}$, and time $\mathscr{T} = \mathscr{L}/\mathscr{U}$, where g is the magnitude of the acceleration due to gravity, $K = a^2/12$ is the permeability, ν is the kinematic viscosity, ϕ is the porosity (taken here as 1), α_A is the solutal expansion coefficient of species A (defined as $\frac{1}{\rho_0}\frac{\partial \rho}{\partial A}$ where ρ_0 is the density of the pure solvent, water in our experiments), and D_A its diffusion coefficient. The concentration was nondimensionalised as $(A - A_b)/(A_t - A_b)$. The initial conditions are $A = 1, \mathbf{u} = \mathbf{0}$ in the upper half and $A = 0, \mathbf{u} = \mathbf{0}$ in the lower half ($y = 0$ is the initial contact line between both liquids). Periodic boundary conditions are used in the horizontal x direction while we impose $\partial A/\partial y = 0, \mathbf{u} = \mathbf{0}$ on $y = \pm \mathrm{Ra}$ where the Rayleigh number $\mathrm{Ra} = \alpha_A A_t g K H/\nu\phi D_A$ only appears here as the location of the upper and lower boundaries [3], where H is the dimensional height of the system.

The parameter-free nondimensional equations (1) explicitly show that, in a sufficiently long numerical domain, i.e., if $\mathrm{Ra} \to \infty$, the dynamics is trivially independent of the Rayleigh number since all the relevant processes arise near the interface and are not affected by walls [13,23,24]. This explains why quantities such as the dissipation rate, the dissolution flux, and other measures

of flow dynamics are seen to converge to constant values in the limit of high Ra in some numerical studies of buoyancy-driven instabilities [2,4]. All numerical results given here are in this limit of parameter-free, large Ra regime. Note that experiments, on the other hand, show dimensional variables that vary with concentrations and solutes chosen and thus with the Rayleigh number. Their trends compare nevertheless favorably with the universal trend predicted by the theory as seen below.

Our numerical simulations have been done using the finite-volume code YALES2 [25]. The RT instability is triggered by introducing a small perturbation on the concentration field throughout the domain (similar to the noise present in the experiments). Validation tests give good agreement between our growth rate and wavelength of the RT fingers computed in the onset regime with theoretical linear stability analysis predictions [13].

Figure 1 shows that, both in experiments and numerical simulations, fingers emerge after a while around the initial contact line. In the beginning, there is a diffusive regime in which the perturbations decay, and the numerical density profile remains close to the diffusive error function. Eventually, the perturbations amplify exponentially due to the unstable density stratification. At a given time, a first rippling of the interface is observed when the instability kicks in. The fingers then convect upwards and downwards in a symmetric way. Note that the gradients of density seen in the numerical simulations are localized along the edges of these fingers, particularly at the upper and lower tips, and that the vertical extent of the fingered zone is roughly constant along the horizontal direction. The next stage is characterized by interactions between fingers with merging and creation of complex shapes. In the experimental snapshots, mushroom-shaped caps are observed at the edges of the fingers during the later stages (Fig. 1, top right). They are not clearly visible in the last numerical panel of Fig. 1 (bottom right). This is due to the fact that numerical simulations show the reconstructed density gradients while experiments visualize refractive index gradients. Even though the two quantities are similar, they are not exactly the same. In particular the details around the zones of sharp refractive index gradients are smoothed out, which explains why the diffusive edges seen in the numerics are not captured in the high-contrast zones visualized experimentally that take hence a mushroom form.

The temporal evolution of the finger mixing length L is shown in Fig. 2. In the numerical simulations, L is defined as the distance between $A = 0.01$ and 0.99 along the transverse direction. As expected, before the instability sets in, a diffusive behavior in which the mixing length grows as $\sqrt{t}$ is observed [referred to as **D**: diffusive in Fig. 2(a)]. Once the instability has set in, the growth rate of the mixing length increases (see **T**: transition regime) and eventually, $L \sim t$ in the nonlinear regime (referred to as **NL**). In numerics, these scalings are universal and independent of Ra, yet the onset time of the convective regime varies with the amplitude of the noise as seen on Fig. 2(b).

A similar transition from a diffusive to a convective regime is obtained in experiments [Fig. 2(b)] where the mixing length L has been computed as the distance between the most upward and downward points of the fingers and normalized by its initial value L_0. Various sets of concentrations and different solutes have been scanned corresponding to various Ra, which leads to different onset times. As in our numerical simulations, the system switches from a diffusive $\sqrt{t}$ regime to a convective t nonlinear regime after a while. In all cases, a constant vertical velocity U can be defined in the nonlinear regime based on the rate of growth of the mixing length as a function of time such that $L \sim Ut$.

Another useful diagnostic to understand the flow dynamics is the average widths of fingers and plumes, $W_A = \pi/k$ [3], where k is defined as

$$k = \sqrt{\langle(\partial A'/\partial x)^2\rangle/\langle(A')^2\rangle}, \tag{2}$$

which is the root mean square of the wave numbers in a Fourier decomposition. Here A' denotes the fluctuations in concentrations defined as $A' = A - \langle A\rangle$, with $\langle A\rangle$ being the horizontally averaged concentration. In Fig. 3(a), the temporal evolution of W_A is measured in our simulations at various heights y in the domain. Initially, only a uniform distribution of perturbations is present such that the initial evolution of W_A varies as $\sqrt{t}$ at each height as the dynamics is first purely diffusive. Once

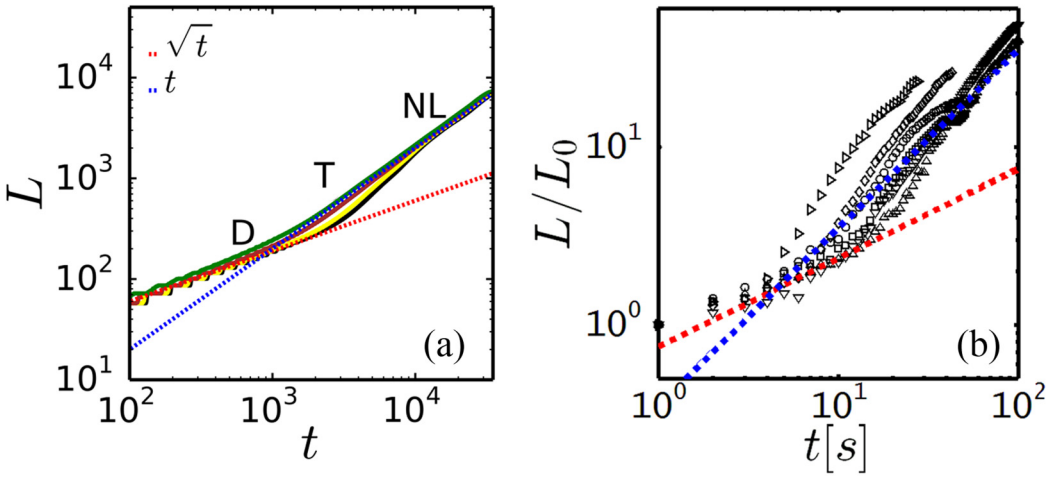

FIG. 2. Mixing length L as a function of time in (a) numerics, averaged over 50 numerical realizations with different amplitudes of initial noise (black: 2%, yellow: 5%, brown: 10%, green: 20%) for Ra = 4096; (b) experiments carried out at different Rayleigh numbers using different solutes or concentrations (◯ NaCl $A_t = 0.73$M, $A_b = 0.417$M, $\alpha_A = 0.04$ l/mol, $D_A = 1.54 \times 10^{-5}$ cm^2/s; □ NaCl $A_t = 0.73$M, $A_b = 0.472$M; ♢ sucrose $A_t = 0.1$M, $A_b = 0.016$M; △ sucrose $A_t = 0.04$M, $A_b = 0.016$M; ▽ sucrose $A_t = 0.06$M, $A_b = 0.0106$M; and ▷ KCl $A_t = 0.772$M, $A_b = 0.324$M, $\alpha_A = 0.048$ l/mol, $D_A = 1.91 \times 10^{-5}$ cm^2/s). The experimental values of the mixing lengths are normalized by their initial value L_0. The red and blue dotted lines correspond to $\sqrt{t}$ and t respectively.

fingers reach a particular height within the domain, the results show that the time dependence of W_A remains nevertheless $\sqrt{t}$.

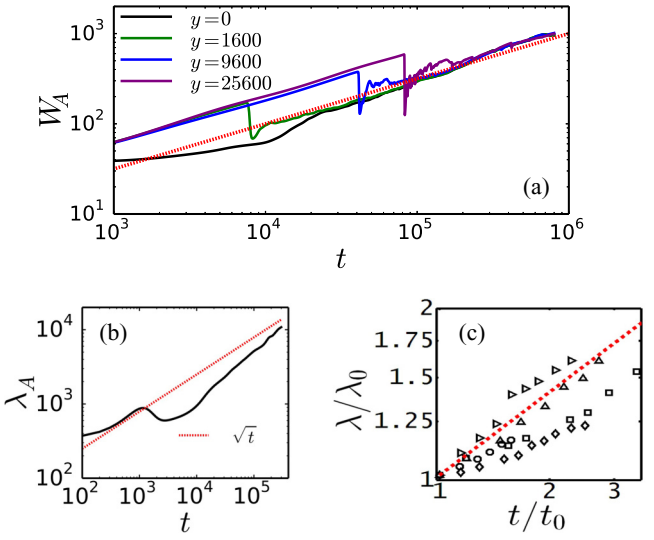

FIG. 3. Temporal evolution of (a) the width of the fingers W_A computed numerically along various horizontal lines at fixed y positions in a single numerical realization (Ra = 51200); (b) the numerical power averaged mean wavelength λ_A; (c) the experimental normalized wavelength (♢ sucrose $A_t = 0.1$M, $A_b = 0.016$M; △ sucrose $A_t = 0.04$M, $A_b = 0.016$M; ▷ KCl $A_t = 0.772$M, $A_b = 0.324$M; ◯ KCl $A_t = 0.154$[M], $A_b = 0.108$[M]; and □ KCl $A_t = 0.404$M, $A_b = 0.05$M). The red line corresponds to $\sqrt{t}$.

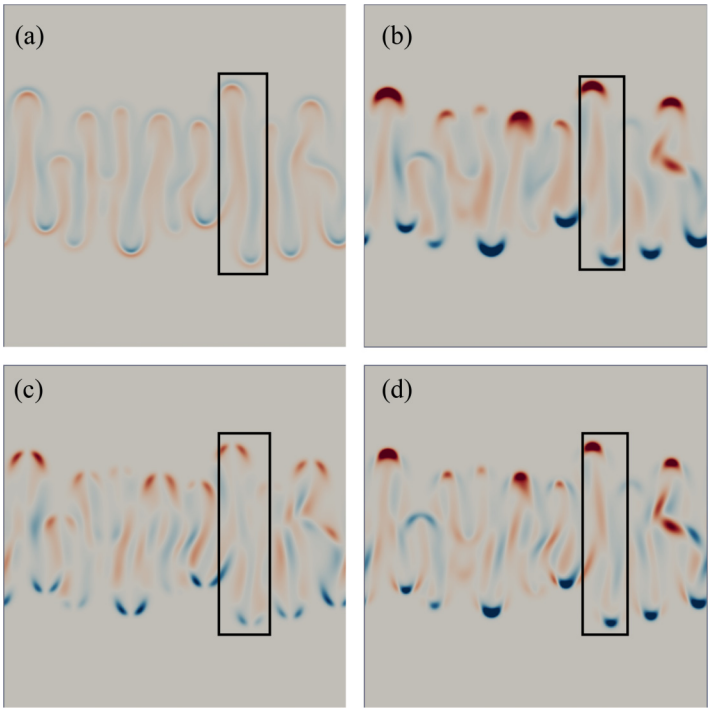

FIG. 4. Spatial distribution of the contributions of diffusion and convection at $t = 13\,000$ with the color map fixed between $[-0.0005, 0.0005]$ as red and blue respectively: (a) $\nabla^2 A$; (b) $\mathbf{U} \cdot \nabla A$; (c) $U_x \partial A/\partial x$; and (d) $U_y \partial A/\partial y$. The black box is chosen to isolate the contribution of convection and diffusion within a single finger.

We also compute the mean wavelength λ_A defined as [26]

$$\lambda_A = 2\pi \frac{\Sigma_i P_i}{\Sigma_i k_i P_i}, \tag{3}$$

where k_i are the Fourier modes of the Fourier transform $\hat{A}(k,t)$ of the numerical transverse averaged profile $\langle A(x,t) \rangle$ and $P(k) = |\hat{A}(k)|^2$ is their amplitude in Fourier space. Its temporal evolution from a single realization in numerics, representative of the general picture, is given in Fig. 3(b). This can be compared to the experimental cases [Fig. 3(c)] where the wavelength is computed as the averaged horizontal distance between the finger tips. In experimental data, the wavelength and time have been rescaled by λ_0 and time t_0, the wavelength and time when a finger is first observed. Note that λ denotes the interplume spacing rather than the width of the plumes and that these two are not necessarily equal. Unfortunately, unlike the mixing length L, the width W_A is a much more difficult quantity to measure experimentally, especially for the case of RT instability due to its rapid evolution accompanied by the merging of fingers.

To interpret the temporal evolution of the mixing length and the width of the fingers, we now compute the relative contribution in the numerical flow dynamics of the diffusive term $\nabla^2 A$, the convective term $\mathbf{u} \cdot \nabla A$, along with the x and y components, $u_x \partial A/\partial x$, and $u_y \partial A/\partial y$ respectively. Figure 4 shows each of these contributions at a given time in the nonlinear regime. Noticeably, we see that the convective term is dominant only at the tips of the fingers. A separate inspection of its horizontal and vertical contributions shows that the vertical component is strongest at the center of the finger tips [Fig. 4(d)], while, as a result of incompressibility, the horizontal component dominates at the outer edges of the fingers [Fig. 4(c)]. The elongation of the fingers in the nonlinear regime is

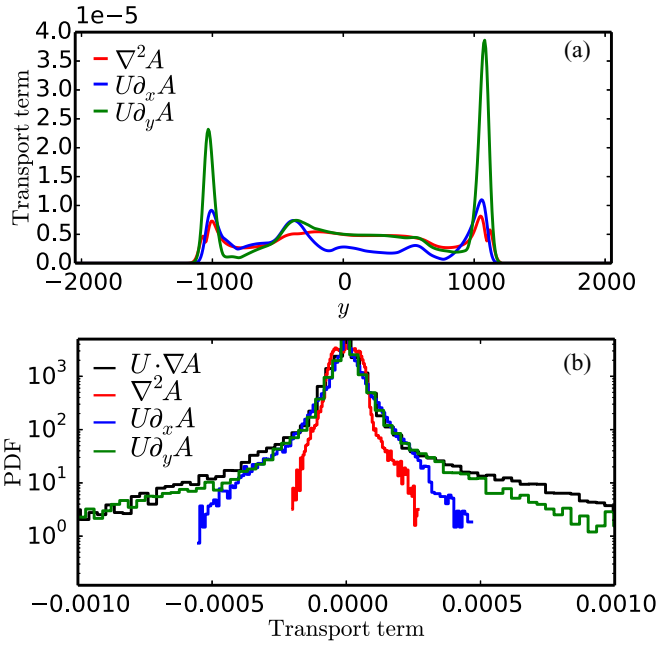

FIG. 5. (a) Horizontally averaged values of diffusive and convective terms along the y axis within the black box shown in Fig. 4. (b) Histograms for the convective term (black), the diffusive term (red), the convective term in the x direction ($u_x \partial A/\partial x$) (blue), and the convective term in the y direction ($u_y \partial A/\partial y$) (green).

thus clearly due to vertical convection at their tips and, as a logical result, the mixing length grows like $L \sim Ut$ as discussed above.

In the bulk of the mixing zone, away from the finger tips, the situation is different. Figure 4 shows that convection and diffusion have similar amplitudes in that region. To better quantify the relative contribution of convection and diffusion within one single finger, we closely inspect the region highlighted using a black box in Fig. 4 that encapsulates a finger in the upward and downward directions. In Fig. 5(a), we plot the intensity in this box of the diffusive term and of the horizontal and vertical components of the convective term, averaged along the horizontal direction. As discussed above, the plot confirms the presence of strong vertical convection at the tips of the fingers. Within the bulk of the domain, the diffusive term dominates the horizontal component of the convective term and is of similar magnitude as the vertical one. Though Fig. 5(a) shows a specific case where the observation has been based on a single finger, the same conclusions have been observed to hold for all the fingers.

To further illustrate this, we have computed in Fig. 5(b) the probability distribution function (PDF) of the diffusive and convective terms (both horizontal and vertical) in the whole domain in Fig. 4. The PDF of the diffusive term corresponds to a Gaussian distribution. This is in contrast with the histograms of the convective terms, which exhibit long tails. These long tails correspond to events located in the fingertips (as confirmed by observing the locations of the corresponding values in Fig. 4). However, in the bulk of the mixing zone (corresponding to low values on the x axis), all transport terms have comparable histograms. Collecting the above observations, we conclude that, away from the fingertips, diffusion is equally important as convection and that it even dominates over lateral convection in this nonlinear regime. As a result, the lateral spreading of the fingers does not depart much from a diffusion dominated process, consistently with the $\sqrt{t}$ time dependence of W_A observed in Fig. 3(a) [3].

In conclusion, we have shown both numerically and experimentally that, in the course of a miscible RT instability in porous media, diffusion contributes in the same way as convection within

the fingered zone, and that the lateral spreading of the fingers remains a diffusion-dominated process. The present work applies to both single species and two species Rayleigh-Taylor instability in porous media. We have demonstrated that diffusion is of the same order of magnitude as convection during the nonlinear regime within the fingered zone. Monitoring only the global contribution of convection and diffusion could be misleading as convection is then indeed globally dominant over diffusion. Instead, inspecting the relative role of convection and diffusion within one isolated finger shows that both transport processes are there of the same order of magnitude within the fingered zone. An excellent agreement between our numerical and experimental observations with respect to the temporal evolution of the mixing length and finger wavelength was achieved. The mixing length evolves as t, showing that in the nonlinear regime a constant vertical velocity U can be defined such that $L \sim Ut$. The width was observed to grow as $\sqrt{t}$. This diffusion-dominated growth has been explained by analyzing the relative contribution of convective and diffusive terms within a finger showing that, away from the fingertips, diffusion is as important as convection, and even dominates over lateral convection.

This demonstrates the need to take diffusive phenomena into account when quantifying specific transport scalings in convective instabilities in porous media. As an example, this might be of importance when estimating the storage capacity of CO_2 sequestration sites or pollution damages in soils when evaluating respective lateral and vertical spreading and mixing scales of injected CO_2 or contaminant plumes. Our analysis has focused here on the Rayleigh-Taylor instability in miscible systems. It will be interesting to verify if our observations remain robust for double-diffusive instabilities [27] and for convective dissolution in partially miscible systems as observed in CO_2 dissolution in aquifers. This will be the subject of further studies.

We thank the Action de Recherches Concertées CONVINCE programme for financial support. J.C.-L. acknowledges support as a F.R.S.-FNRS Fellow. The present research benefited from computational resources made available on the Tier-1 supercomputer of the Fédération Wallonie-Bruxelles, infrastructure funded by the Walloon Region under Grant Agreement No. 1117545.

[1] C. T. Tan and G. M. Homsy, Simulation of nonlinear viscous fingering in miscible displacement, Phys. Fluids **31**, 1330 (1988).

[2] J. J. Hidalgo, J. Fe, L. Cueto-Felgueroso, and R. Juanes, Scaling of Convective Mixing in Porous Media, Phys. Rev. Lett. **109**, 264503 (2012).

[3] A. C. Slim, Solutal-convection regimes in a two-dimensional porous medium, J. Fluid Mech. **741**, 461 (2014).

[4] P. Jenny, J. S. Lee, D. W. Meyer, and H. A. Tchelepi, Scale analysis of miscible density-driven convection in porous media, J. Fluid Mech. **749**, 519 (2014).

[5] D. R. Hewitt, J. A. Neufeld, and J. R. Lister, Ultimate Regime of High Rayleigh Number Convection in a Porous Medium, Phys. Rev. Lett. **108**, 224503 (2012).

[6] M. Sajjadi and J. Azaiez, Scaling and unified characterization of flow instabilities in layered heterogeneous porous media, Phys. Rev. E **88**, 033017 (2013).

[7] I. Bischofberger, R. Ramachandran, and S. R. Nagel, Fingering versus stability in the limit of zero interfacial tension, Nat. Commun. **5**, 5265 (2014).

[8] S. Backhaus, K. Turitsyn, and R. E. Ecke, Convective Instability and Mass Transport of Diffusion Layers in a Hele-Shaw Geometry, Phys. Rev. Lett. **106**, 104501 (2011).

[9] P. A. Tsai, K. Riesing, and H. A. Stone, Density-driven convection enhanced by an inclined boundary: Implications for geological CO_2 storage, Phys. Rev. E **87**, 011003(R) (2013).

[10] V. Loodts, C. Thomas, L. Rongy, and A. De Wit, Control of Convective Dissolution by Chemical Reactions: General Classification and Application to CO_2 Dissolution in Reactive Aqueous Solutions, Phys. Rev. Lett. **113**, 114501 (2014).

[11] A. Traxler, P. Garaud, and S. Stellmach, Numerically determined transport laws for fingering ("thermohaline") convection in astrophysics, Astrophys. J. Lett. **728**, L29 (2011).

[12] W. H. Cabot and A. W. Cook, Reynolds number effects on Rayleigh-Taylor instability with possible implications for type-1a supernovae, Nat. Phys. **2**, 562 (2006).
[13] P. M. J. Trevelyan, C. Almarcha, and A. De Wit, Buoyancy-driven instabilities of miscible two-layer stratifications in porous media and Hele-Shaw cells, J. Fluid Mech. **670**, 38 (2011).
[14] T. Menand and A. W. Woods, Dispersion, scale, and time dependence of mixing zones under gravitationally stable and unstable displacements in porous media, Water Resour. Res. **41**, W05014 (2005).
[15] J. W. Elder, The unstable thermal interface, J. Fluid Mech. **32**, 69 (1968).
[16] T. Radko, *Double Diffusive Convection* (Cambridge University Press, Cambridge, UK, 2013).
[17] J. S. Turner, *Buoyancy Effects in Fluids* (Cambridge University Press, Cambridge, UK, 1979).
[18] J. Fernandez, P. Kurowski, P. Petitjeans, and E. Meiburg, Density-driven unstable flows of miscible fluids in a Hele-Shaw cell, J. Fluid Mech. **451**, 239 (2002).
[19] J. Carballido-Landeira, P. M. J. Trevelyan, C. Almarcha, and A. De Wit, Mixed-mode instability of a miscible interface due to coupling between Rayleigh-Taylor and double-diffusive convective modes, Phys. Fluids **25**, 024107 (2013).
[20] Y. Shi and K. Eckert, A novel Hele-Shaw cell design for the analysis of hydrodynamic instabilities in liquid-liquid systems, Chem. Eng. Sci. **63**, 3560 (2008).
[21] G. S. Settles, *Schlieren and Shadowgraph Techniques* (Springer, Berlin, 2001).
[22] E. Guyon, J.-P. Hulin, L. Petit, and C. Mitescu, *Physical Hydrodynamics* (Oxford University Press, Oxford, UK, 2001).
[23] A. De Wit, Fingering of Chemical Fronts in Porous Media, Phys. Rev. Lett. **87**, 054502 (2001).
[24] O. Manickam and G. M. Homsy, Fingering instabilities in vertical miscible displacement flows in porous media, J. Fluid Mech. **288**, 75 (1995).
[25] V. Moureau, P. Domingo, and L. Vervisch, Design of a massively parallel CFD code for complex geometries, C. R. Mécanique **339**, 141 (2011).
[26] A. De Wit, Miscible density fingering of chemical fronts in porous media: Nonlinear simulations, Phys. Fluids **16**, 163 (2004).
[27] Y. Luo and Y. Gong, Comparative study of buoyancy-driven instability for thermohaline stratification in a Hele-Shaw cell and extended geometry, Eng. Appl. Comput. Fluid Mech. **9**, 469 (2015).